

Failure of Multilayer Suspension Plasma Sprayed Thermal Barrier Coatings in the Presence of Na₂SO₄ and NaCl at 900 °C

Krishna Praveen Jonnalagadda¹ · Satyapal Mahade² · Stephanie Kramer¹ · Pimin Zhang¹ · Nicholas Curry³ · Xin-Hai Li⁴ · Ru Lin Peng¹

Submitted: 19 June 2018 / in revised form: 6 September 2018 / Published online: 29 October 2018
© The Author(s) 2018

Abstract The current investigation focuses on understanding the influence of a columnar microstructure and a sealing layer on the corrosion behavior of suspension plasma sprayed thermal barrier coatings (TBCs). Two different TBC systems were studied in this work. First is a double layer made of a composite of gadolinium zirconate + yttria stabilized zirconia (YSZ) deposited on top of YSZ. Second is a triple layer made of dense gadolinium zirconate deposited on top of gadolinium zirconate + YSZ over YSZ. Cyclic corrosion tests were conducted between 25 and 900 °C with an exposure time of 8 h at 900 °C. 75 wt.% Na₂SO₄ + 25 wt.% NaCl were used as the corrosive salts at a concentration of 6 mg/cm². Scanning electron microscopy analysis of the samples' cross sections showed that severe bond coat degradation had taken place for both the TBC systems, and the extent of bond coat degradation was relatively higher in the triple-layer system. It is believed that the sealing layer in the triple-layer system reduced the number of infiltration channels for the molten salts which resulted in overflowing of the salts to

the sample edges and caused damage to develop relatively more from the edge.

Keywords columnar microstructure · composite of gadolinium zirconate and YSZ · hot corrosion · suspension plasma spray

Introduction

Suspension plasma spray (SPS) is a recent advancement in thermal barrier coatings deposition (Ref 1, 2). Thermal barrier coatings (TBCs), typically having a bi-layer structure with metallic layer and a ceramic top layer, are used in the hot sections of gas turbines and in diesel engines to provide components with resistance against high-temperature degradation (Ref 3-8). SPS TBCs offer a low-cost alternative to the more established, yet expensive, electron-beam physical vapor deposition (EB-PVD) TBCs. The main advantage of SPS deposition technique is its ability to provide a vertical columnar structure as in EB-PVD as well as a compact horizontal structure by changing the process parameters (Ref 9, 10). The vertical columnar structure is believed to have a superior strain tolerance during thermal cycling than by other low-cost coating deposition techniques like atmospheric plasma spraying (Ref 11).

The choice of material for the coating deposition can have a significant influence on the coating performance at high temperatures. Although yttria stabilized zirconia (YSZ), with its attractive properties, is still the industry standard for the topcoat material, the recent focus has been on other materials that can circumvent the limitations of conventional YSZ, for instance, the high-temperature phase stability of YSZ (Ref 12, 13). Among all the materials being researched for the topcoat layer in TBCs,

This article is an invited paper selected from presentations at the 2018 International Thermal Spray Conference, held May 7-10, 2018, in Orlando, Florida, USA, and has been expanded from the original presentation.

✉ Krishna Praveen Jonnalagadda
praveen.jonnalagadda@liu.se

¹ Department of Management and Engineering, Linköping University, 581 83 Linköping, Sweden

² Department of Engineering Science, University West, Trollhättan, Sweden

³ Treibacher Industrie AG, Althofen, Austria

⁴ Siemens Industrial Turbomachinery AB, 61283 Finspång, Sweden

pyrochlores of $A_2B_2O_7$ -type like lanthanum zirconate and gadolinium zirconate are considered to be potential candidates for the topcoat layer due to their low thermal conductivity and excellent high-temperature phase stability (Ref 14, 15). While the rare earth-based zirconates of lanthanum and gadolinium outperform YSZ when it comes to certain properties like low thermal conductivity and high-temperature phase stability (Ref 14), there is only a limited amount of data available for these materials on their performance during corrosion. Lanthanum zirconate TBCs exhibit minor damage in the presence of vanadium pentoxide while it degrades severely in the presence of sulfates of sodium and magnesium (Ref 16). Lanthanum zirconate is also known to have processing issues during which the material tends to lose its stoichiometry (Ref 17, 18). Gadolinium zirconate, deposited by SPS, on the other hand, has shown to be more susceptible to corrosion-induced damage when exposed to a salt mixture of vanadium pentoxide and sodium sulfate (Ref 19). The main degradation came from attack by the vanadium, and it was also reported in the literature that no direct chemical reaction between gadolinium zirconate and sodium sulfate was known (Ref 20). This makes gadolinium zirconate better resistant to the sulfate environments. However, when gadolinium zirconate is deposited using SPS technique, a columnar microstructure can be generated (Ref 21). The columnar microstructure, with its columnar gaps, likely has effective pathways for the molten salts, and the salts can easily reach the bond coat. The sulfates are known to degrade the bond coat material, which is typical of MCrAlY type (M is Ni and/or Co) (Ref 22, 23). Another limitation with gadolinium zirconate is its thermochemical incompatibility with the thermally grown oxide, alumina (Ref 24). This led to the development of multilayered coatings which were proven to have a better life during thermal cycling than single-layered TBCs (Ref 25–27). Gadolinium zirconate is also known to have lower fracture toughness compared to YSZ (Ref 28). This makes crack propagation much easier in gadolinium zirconate. A novel approach that was developed is to blend gadolinium zirconate and YSZ to make a composite of gadolinium zirconate and YSZ and to deposit this composite on the top of YSZ. A composite of gadolinium zirconate and YSZ has shown to have better resistance against corrosion-induced damage than pure gadolinium zirconate in the presence of V_2O_5 and Na_2SO_4 (Ref 21). It is of interest to understand how such a coating performs in the presence of a salt mixture of sodium sulfate and sodium chloride. The environment with sulfates and chlorides of sodium is common during the operation of land-based gas turbines used specially for offshore applications. As per the best of authors' knowledge, no such work has been published before and understanding the performance of these coating systems in

the presence of a salt mixture of sodium sulfate and sodium chloride is the focus of the current investigation. The term gadolinium zirconate is abbreviated as GZ hereafter.

Two coating systems, a double-layer composite of GZ + YSZ/YSZ, and a triple-layer, dense GZ (DGZ)/GZ + YSZ/YSZ are studied in this work. The expected purpose of the dense layer is to seal the columnar gaps which could have an influence on the corrosion resistance. The corrosion behavior on the TBC system as a whole is studied in this work.

Experiment

Materials

Hastelloy[®] X in the form of disks with a diameter of 25.4 mm and thickness of 6.35 mm was used as the substrate in the present work. The substrate disks were grit blasted using alumina of 220 grit size prior to bond coat deposition to achieve a surface roughness, R_a , value of 3 μm . An MCrAlY-type bond coat, Amdry 386 with nominal composition of Ni18Co13Cr10Al0.1Y was deposited on the substrates using a M3 gun (UniqueCoat, Virginia, USA) by the high-velocity air fuel (HVOF) process.

For the top coat, three different suspensions (1 commercial and 2 experimental) manufactured by Treibacher Industrie AG (Althofen, Austria) were used in this work. The first suspension was an ethanol-based commercially available AuerCoat YSZ suspension, which had a mean particle diameter of 500 nm and a solid load content of 25 wt.%. The second suspension was an experimental type ethanol-based suspension comprising of a 50:50 wt.% mixture of GZ and YSZ. The mean particle diameter was 500 nm, and the solid load in the suspension was kept at 25 wt.%. The third is an experimental type water-based suspension comprising of GZ with a mean particle size of approximately 500 nm and the solid load content of 40 wt.%. The reason for using a 40% solid load water-based suspension was to alter the viscosity and surface tension. A higher viscosity and surface tension of the solvent lead to relatively poor atomization of the suspension droplet which eventually results in a denser coating deposition (Ref 29). The suspensions were kept on rollers overnight to obtain good dispersion of the solute in the suspension.

The bond-coated substrates were preheated prior to the topcoat deposition. Preheating of the bond-coated substrates was carried out using the Axial III Mettech gun which was operated without the suspension. The surface temperature of the bond coat was maintained at approximately 200 °C during the preheating. Preheating could help to remove the volatile dirt from the surface. Top coats were

deposited using a Axial III Mettech gun (Mettech Corp, Vancouver, Canada). The spray process was stopped for about 30 min after the deposition of each layer (YSZ, GZ + YSZ, and dense GZ, respectively) to change the suspension in the feeding system for the subsequent layer. The start and stop of the spray process during a multiceramic layered TBC deposition could result in discontinuity of the TBC due to horizontal cracks at the interface of each new layer. However, in this work, before the start of each new layer deposition, the surface was preheated in order to ensure continuity of the layers and horizontal crack-free interface. Further details regarding the deposition process can be found in our previous work (Ref 21).

Corrosion Tests

Corrosion tests were conducted with a salt mixture of 75 wt.% Na_2SO_4 + 25 wt.% NaCl at a concentration of 6 mg/cm². The salt mixture was spread on the surface of the sample evenly without touching the edges (a clearance of 3 mm from the sample's edge was maintained). The samples were later placed in a furnace preheated to 900 °C. The samples were held at the test temperature for 8 h after which they were removed from the furnace and allowed to cool in atmosphere (~ 80 min) till they reached the room temperature (~ 25 °C). The exposure time and cooling together constituted one corrosion cycle.

After each corrosion cycle, the samples were visually inspected and photographed using a consumer grade camera under identical lighting conditions. The salts were spread again on the sample's surface and a new cycle was started. The testing was continued until the samples' top surface showed a damage of about 75%, and the samples were judged to have failed. Damage in this context is defined as visible spallation of the top coat, and the arbitrary value of 75% was selected so that both undamaged and damaged regions in the cross sections could be observed. In the present case, approximately 75% failure value was observed after 24 corrosion cycles for both the coating systems. After the first round of corrosion tests, a set of new samples was subjected to the interrupted corrosion test cycles during which the samples were tested till the damage first started to appear (9 cycles for both the samples. See Fig. 1). This was done to understand the damage development in both the coating systems.

Characterization

The tested samples were investigated in an x-ray diffractometer (X'pert Pro, Pan Analytical) with Cu as the source ($K_\alpha = 0.154$ nm). The samples were later infiltrated with

epoxy under vacuum to prevent damage to the coating during the subsequent stages of sample preparation. The samples were thereafter cut along the diameter to reveal the cross-section and prepared for cross-sectional analysis in a scanning electron microscope (SEM) according to the normal routine for the thermal barrier coating sample preparation described in (Ref 30). Energy-dispersive x-ray spectroscopy (EDS) was used to identify the elements in the coating's cross-section.

Results

Selected Visual Images of the Samples During Corrosion

Figure 1 shows selected visual images of the double-(GZ + YSZ/YSZ) and triple-layer (DGZ/GZ + YSZ/YSZ) samples during the different stages of corrosion. The typical salt spread region after the first and fifth cycle is marked with the black lines in the double-layer system. As shown in Fig. 1, the salt coverage is roughly circular. For up to 9 corrosion cycles, the top surface appeared to be free from damage. After the ninth cycle, the damage started to increase slowly from the edges and started to propagate toward the center. After 24 cycles, for both the double- and triple-layer samples, the visible damage was estimated at about 75% of the topcoat surface and the tests were stopped. Just with the visual inspection, there appeared to be no significant difference in the extent of damage between the double- and triple-layer samples. It has to be noted that even though there is no significant difference in the radial direction during visual inspection, there could be difference in the Z-direction (thickness) of the damaged regions. This is very difficult to observe just with visual inspection. It is emphasized here that the purpose of visual inspection, through a camera, is to illustrate the damage development from the edge to the coating center with increased exposure time. Accurate and more in-depth analysis of the coatings' cross section was obtained from SEM analysis (discussed in the subsequent sections).

As-Received Samples Before Corrosion Tests

Figure 2(a)–(c) shows the SEM images of the as-received double-layer (see Fig. 2a) and triple-layer (see Fig. 2b) coating systems, respectively. The nominal thickness of YSZ layer is 40 μm , GZ + YSZ layer is 210 μm , and the DGZ layer is 30 μm . Columnar structure for YSZ and GZ + YSZ layer can be observed. The third layer (DGZ) is compact and does not have a columnar structure. Fig-

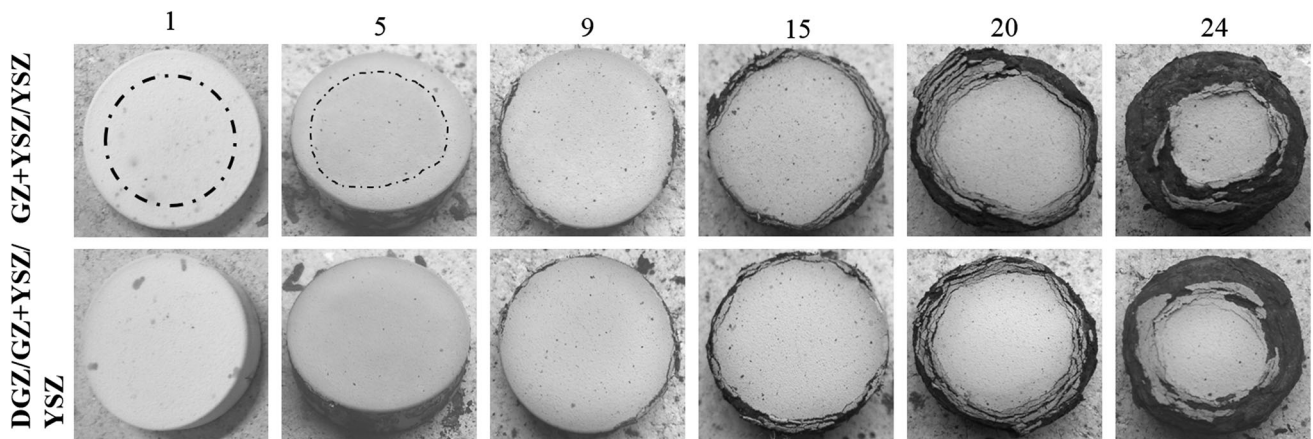


Fig. 1 Selected visual images showing the top surface of the two TBC systems after different corrosion test cycles. The salt spread region is approximately marked using a black dash-dot line after cycles 1 and 5

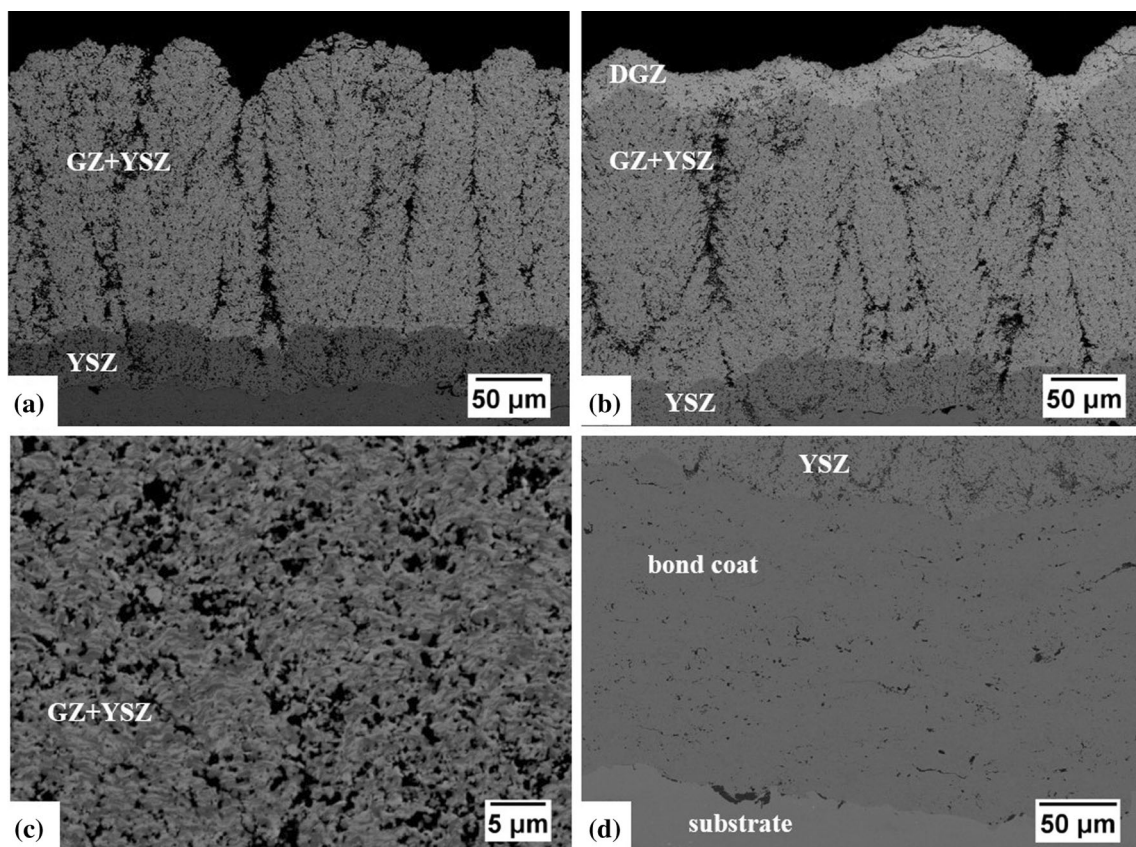


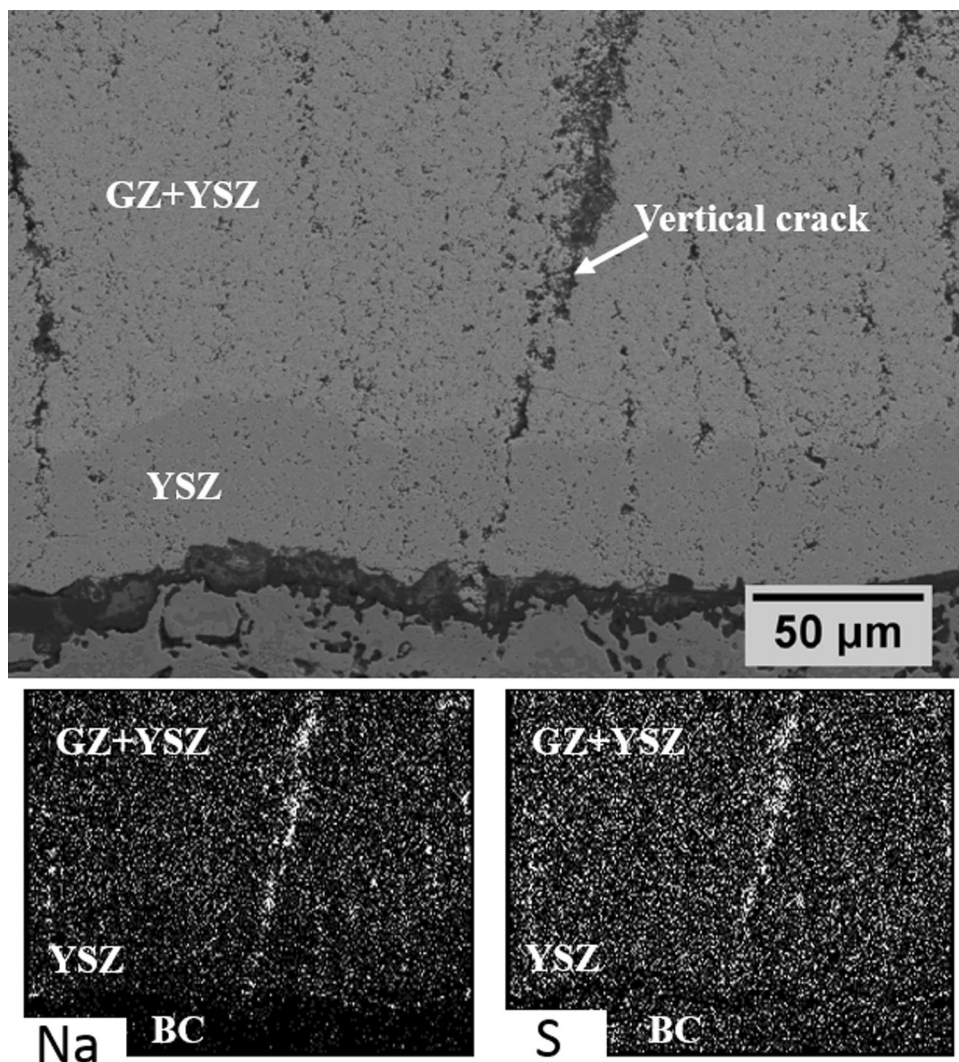
Fig. 2 Cross-sectional SEM images of as-received (a) double-layer GZ + YSZ/YSZ, (b) triple-layer DGZ/GZ + YSZ/YSZ, (c) high magnification image of GZ + YSZ in (a), and (d) bond coat

ure 2(c) shows the high magnification image of the GZ + YSZ layer where both the gadolinium zirconate and yttria-stabilized zirconia are present. Figure 2(d) shows the HVAF sprayed bond coat layer with a dense microstructure. Good bond coat/YSZ, YSZ/GZ + YSZ and GZ + YSZ/DGZ interface, free from cracks, were observed.

Double-Layer (GZ + YSZ/YSZ) System After 24 Cycles

Figure 3 shows the infiltration of the molten corrosive salts through the columnar gaps along with the EDS maps revealing the presence of sodium (Na) and sulfur (S) in the columnar gaps. There is no reported direct chemical

Fig. 3 SEM image showing the infiltration of the molten salts through the vertical cracks (columnar gaps) in the topcoat along with the EDS maps for sodium (Na) and sulfur (S). It has to be noted that the boundary between the BC/YSZ/GZ + YSZ layer is not visible in the EDS maps



reaction between GZ and sodium sulfate at high temperatures (Ref 20). The molten salts infiltrate through the columnar gaps between the columns and reach and attack the bond coat material (represented by white arrow) as indicated in Fig. 3. At the same time, some molten salts overflow from the top surface to the edge and then to the side surface and react with the substrate material, as shown in Fig. 1. This results in the degradation of the substrate and substrate/bond coat interface from the side surface and will lead to damage that can start at the edge and subsequently propagate to the center of the coating.

The cross-sectional SEM images of GZ + YSZ/YSZ coating after 24 corrosion cycles are presented in Fig. 4(a)–(f). The edge of the coating is shown in Fig. 4(a) along with a better view of the edge indicated by region “I” at the bottom left side of Fig. 4(a). Reaction of the molten salts with the substrate and the bond coat at the side surface resulted in severe damage at the edge and the damage started to develop in the bond coat from the edge toward the

center. This damage in the bond coat had resulted in the loss of integrity of the topcoat with the TBC system at the edge (see Fig. 4a). The bond coat degradation from the edge to the center can be observed from Fig. 4(b). The region denoted as “I” which is enlarged in the inset of Fig. 4(b), clearly illustrates the BC degradation with the formation of internal oxides of chromium and aluminum, indicated by the black and white arrows, respectively. The extent of bond coat degradation, in this context, is defined as the depth of internal oxidation expressed in terms of percentage of the total bond coat thickness. The depletion of the β (NiAl) phase roughly follows the bond coat degradation, i.e., the region to the left in Fig. 4(b) still has β phase remaining in the coating (indicated by the double-headed blue arrow). Figure 4(c) shows the microstructure at the center of the coating. The infiltrated molten salts stayed between the columns and resulted in the fluxing of the thermally grown oxide (TGO), alumina. Fluxing of the alumina scale damages the TGO and the salts reach the bond coat surface. The

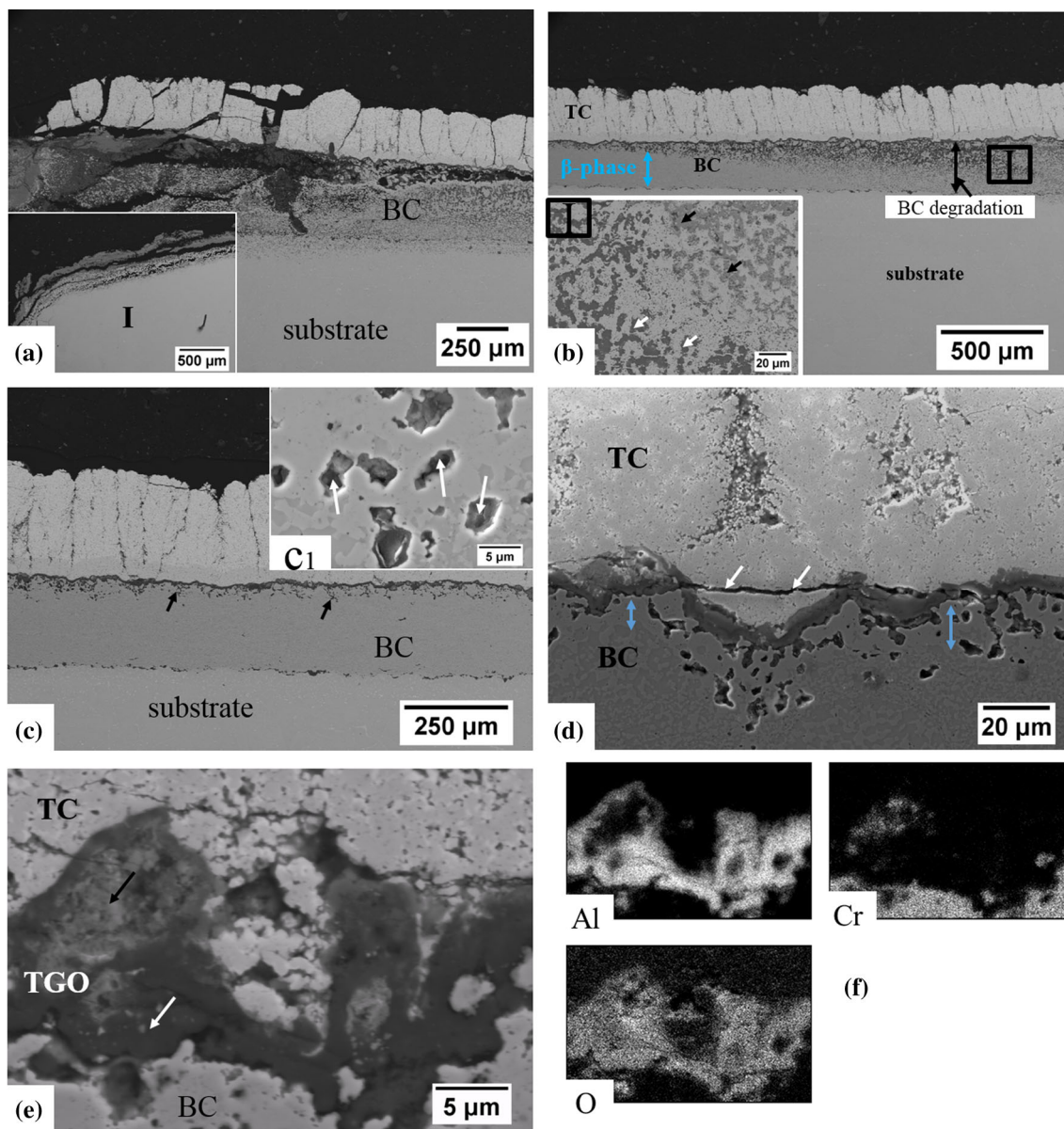


Fig. 4 Cross-sectional SEM images of GZ + YSZ/YSZ (a) coating edge, (b) coating cross section from the edge to the center showing bond coat degradation, (c) coating center, and (d) TGO/topcoat

interface, (e) high magnification image of the TGO, and (f) corresponding EDS maps for (e)

attack on the bond coat resulted in the internal oxidation of alumina along with the presence of some voids indicated by the white arrows as shown in the inset at the top right of Fig. 4(c) (c1). The TGO layer was observed to be a mixture of aluminum and chromium oxides [for instance, see Fig. 4(e) and the corresponding EDS maps in Fig. 4(f)]. The black and white arrows in Fig. 4(e) correspond to chromium and aluminum oxides, respectively. The reaction between the corrosive salts and the TGO can cause a fast growth of the alumina scale due to fluxing. During the cooling part of the corrosion cycle, due to the coefficient of thermal expansion (CTE) mismatch, horizontal cracks as

shown in Fig. 4(d) with white arrows were observed all along the cross section. The depletion of β phase below the TGO is indicated by the double-headed light blue arrows. To summarize, the damage occurred from two fronts in the double-layer sample. First, the damage from the edge degraded the bond coat and damaged the integrity of the top coat. Second, the damage due to the molten salt infiltration caused the fluxing of the alumina scale and promoted rapid growth of alumina and a mixture of alumina and chromia at certain locations. This, in turn, increases the thermal stresses during cooling and promotes crack propagation at the TGO/topcoat interface.

Triple-Layer (DGZ/GZ + YSZ/YSZ) System After 24 Cycles

Figure 5(a)–(c) shows the cross-sectional SEM images of the triple-layer DGZ/GZ + YSZ/YSZ coating system after 24 corrosion cycles. The coating edge is shown in Fig. 5(a), where severe damage had occurred and resulted in the loss of the integrity of the top coat/bond coat with the TBC system. Figure 5(b) shows the microstructure at the center of the coating. Unlike the double-layer system (see Fig. 4c), the extent of bond coat degradation is throughout the coating cross section and also throughout the coating thickness. Figure 5(c) shows a high magnification SEM image at the coating center of the internal oxides (indicated by the white arrows) that are formed in the coating.

Interrupted Corrosion Tests-9 Cycles

Figure 6(a)–(d) shows the cross-sectional SEM images after the interrupted corrosion tests at cycle 9. Damage development from the edge to the center was observed for both the double-layer (see Fig. 6a) and triple-layer (see Fig. 6c) coating systems. Damage is indicated by black arrows in both images. The microstructure of the coatings at the center is shown in Fig. 6(b) and (d) for the double-

and triple-layer systems, respectively. High magnification images of the TGO at the coating center are shown in the insets of Fig. 6(b) and (d). The extent of bond coat degradation is very low and similar for both coating systems. The formed internal oxides are indicated by blue arrows.

Comparison Between GZ + YSZ/YSZ and DGZ/GZ + YSZ/YSZ Coating Systems

Figure 7 shows the extent of bond coat degradation along the diametrical cross section (edge to edge) for the double- (represented by solid red markers) and triple- (represented by solid blue markers)-layer coating systems after 24 corrosion cycles. For 9 corrosion cycles (hollow red and blue markers), the bond coat degradation is only shown from one edge till the center of the coating as the other edge exhibited a similar degradation profile. This was true for both coating systems. From Fig. 7, after 9 corrosion cycles, the degradation profiles were nearly identical for both the double- and triple-layer systems. The extent of degradation was 100% percent at the edge (the entire thickness of bond coat was damaged at the edges) and it dropped to ~ 10% about 1.5 mm from the edge and was then similar till the center of the coating. After 24 corrosion cycles, the bond

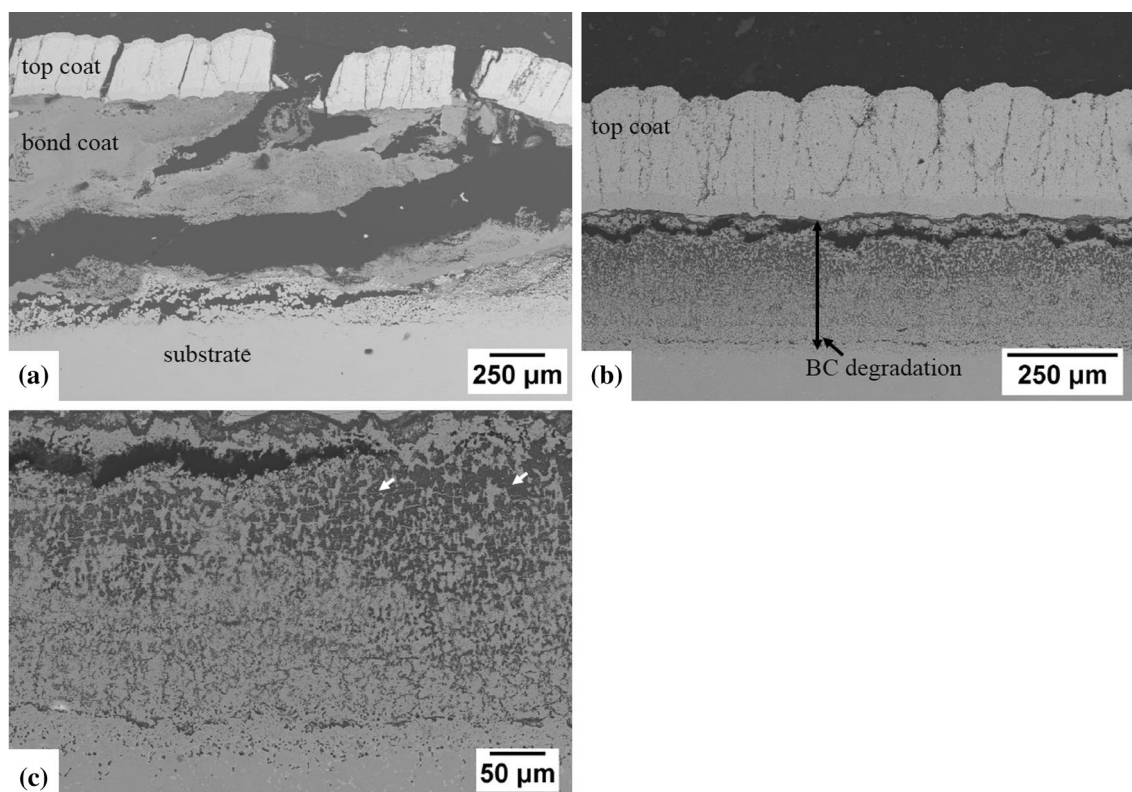


Fig. 5 Cross-sectional SEM images of DGZ/GZ + YSZ/YSZ (a) coating edge, (b) coating cross section at the center showing bond coat degradation, and (c) bond coat degradation at high magnification at the center

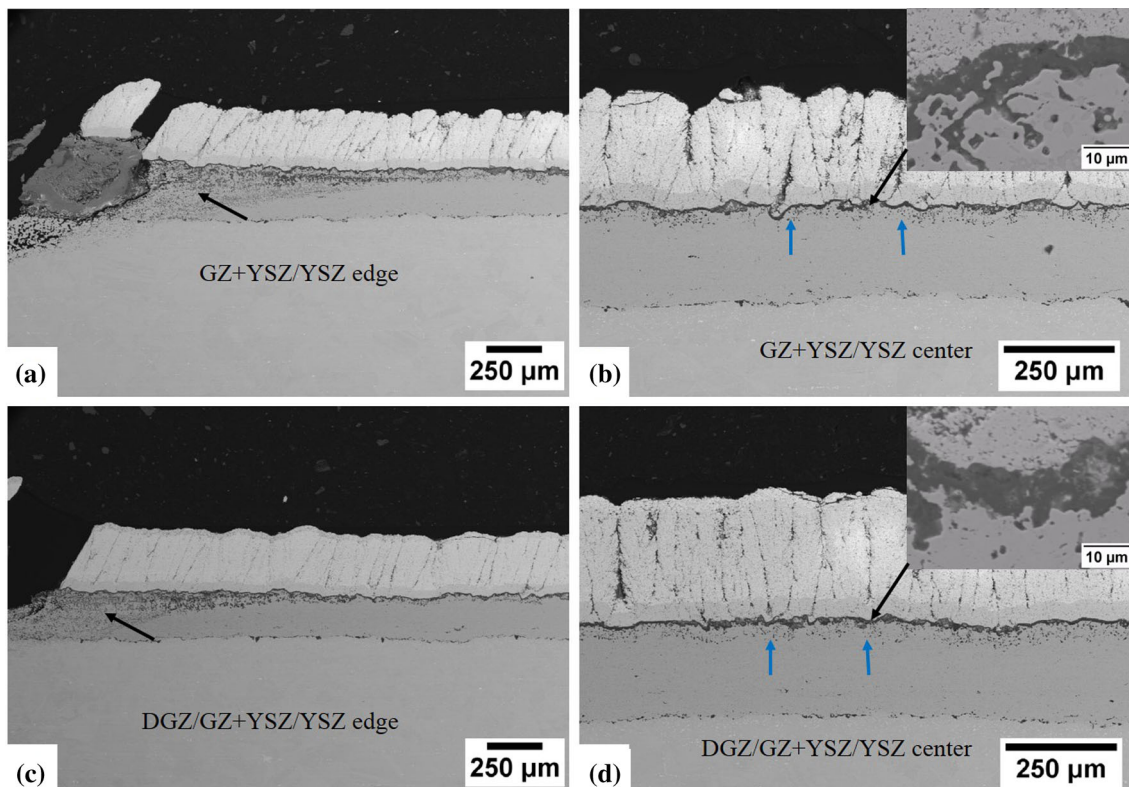


Fig. 6 Cross-sectional SEM images after 9 corrosion cycles showing (a) GZ + YSZ/YSZ edge, (b) GZ + YSZ/YSZ center, (c) DGZ/ GZ + YSZ/YSZ edge, and (d) DGZ/GZ + YSZ/YSZ center

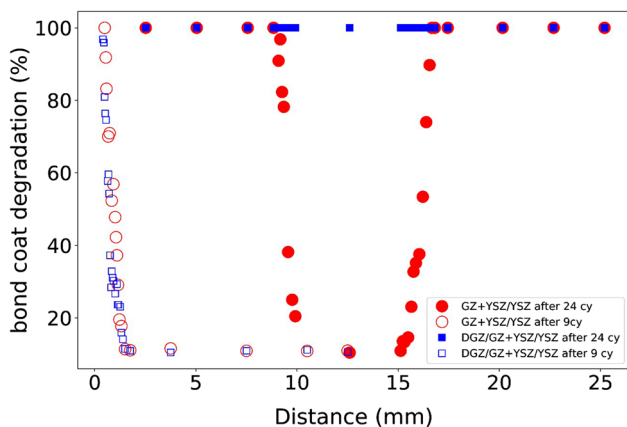


Fig. 7 Profile of bond coat degradation across the diameter (25 mm) in both coating systems after 9 cycles and 24 cycles, respectively

coat degradation in the double-layer system was 100% for about 10 mm from the edge and then it dropped to about 10%. The extent of bond coat damage at the center was observed to be similar after 9 and 24 corrosion cycles. One probable reason could be due to the retention of the molten salts in the columnar gaps, which then limited the exposure of the bond coat surface to new melt. However, the damage from the edge had developed almost to the center of the coating. For the triple-layer system, the entire thickness of

the bond coat had been degraded 100% along the cross section of the coating. As the damage at the center was similar after 9 corrosion cycles for both TBC systems, the contribution of damage from the edge is relatively higher for the triple-layer system. With continued salt exposure (an additional few corrosion cycles), the degradation profile for the double-layer system would be similar to the triple-layer system.

X-ray Diffraction Before and After Corrosion

Figure 8 shows the x-ray diffraction pattern for both the double- and triple-layer systems in their as-sprayed state and after 24 corrosion cycles. The obtained peaks from the XRD were labeled using PDF standards. For the double-layer composite TBC, in its as-sprayed condition, both tetragonal YSZ and cubic defect fluorite gadolinium zirconate phases were observed. This is desirable as the purpose of the composite TBC was to achieve the best properties of both materials such as the fracture toughness of YSZ and low thermal conductivity of gadolinium zirconate. For the triple-layer system, the observed phase on the sealing top layer was defect fluorite of gadolinium zirconate. This phase is a disordered variation of the cubic pyrochlore phase of gadolinium zirconate and is a desired

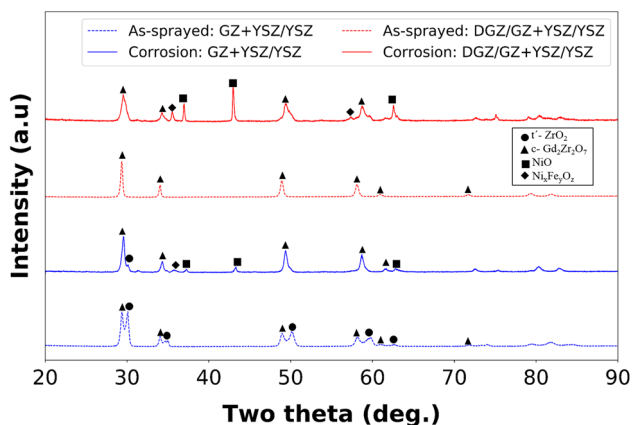


Fig. 8 X-ray diffraction pattern for the samples before and after the corrosion tests

phase for gadolinium zirconate coatings as it is stable up to its melting temperature range.

After the 24 corrosion cycles in the double-layer coating, parts of the original phases (tetragonal zirconia and cubic gadolinium zirconate) were retained in the top coat. The other observed phases were oxides of Ni (NiO) and other compounds of Ni ($\text{Ni}_x\text{Fe}_y\text{O}_z$). As most of the coating was damaged, these phases come from the damaged parts of the coating. The top surface at the center of the coating (see Fig. 1) appeared to be unaffected based on the color of the coating compared to the as-sprayed samples' top surface. At this location, the main phases of the original coating were still retained. This further proves that there is no direct reaction of the corrosive salts with both gadolinium zirconate and yttria-stabilized zirconia. Similar phases, although with different intensities, were observed with the triple-layer DGZ/GZ + YSZ/YSZ coating system. The higher intensity of the NiO signals in the triple-layer system could be because there was relatively more damage from the edge and this could have resulted in higher amounts of corrosion products at the edge compared to the double-layer system.

Discussion

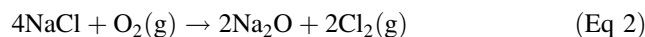
Hot corrosion of coatings in the presence of molten salts can be considered as a form of accelerated oxidation. Corrosion of coatings, in general, has been studied extensively and reported by other researchers (Ref 31–37). Exposure of coatings to high-temperature results in the formation of the protective TGO, α -alumina. In the case of pure oxidation, the growth of alumina scale is parabolic. The alumina scale formation is controlled by the diffusion of aluminum and oxygen along the grain boundary. During exposure to corrosive salts, the thickness of Al depletion

zone was reported to follow an almost linear trend, indicating that the growth of alumina scale is different during the corrosion process (Ref 35). In the present work, the formed alumina scale is under stress due to thermal cycling of the samples (when the samples are cooled in the atmosphere to room temperature), resulting in horizontal cracks at the TGO/topcoat interface (see Fig. 4d). In addition to that, reaction with the salts could result in the alumina dissolution. Consequently, new alumina scale is formed to repair the damaged oxide scale due to both the thermal stress and dissolution. When the continuous alumina scale can no longer be formed, the salts can react directly with the bond coat and result in rapid degradation (Ref 36). Presence of chlorine, in the form of NaCl further accelerates the corrosion by forming internal voids by means of oxychlorination and chlorination/oxidation cyclic reactions (Ref 36). Salt mixtures containing NaCl can cause more severe damage compared to pure Na_2SO_4 (Ref 23).

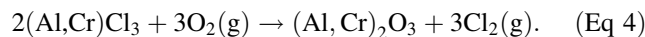
The basic corrosion mechanism is explained below. The initially formed α -alumina at the bond coat/topcoat interface is protective against corrosive salts. With increasing exposure time, the basicity of the molten salt increases and when it reaches a certain value, basic fluxing of alumina scale occurs according to reaction (1) below. If the basic fluxing is sufficiently strong, then the alumina scale will lose its integrity (Ref 23)



Sodium chloride participates in corrosion by reacting with oxygen at high temperatures according to reaction (2) which releases chlorine (Ref 23)



The released chlorine can react with either Al or Cr in the bond coat and form their respective chlorides which are volatile (according to reaction (3)). It was reported that these volatile chlorides can evaporate to the surface leaving voids in the coating (see the insert in Fig. 4c) and when encountering oxygen with higher partial pressure, they can re-oxidize to form oxides of aluminum and chromium (see Fig. 4b, c and 5b, c). The reaction is shown in reaction (4) (Ref 22, 37). This process releases chlorine again which will react with Al/Cr according to reaction (3). The corrosion continues until the entire bond coat has been oxidized or in other words degraded



The focus of this work has been to understand the influence of an inert columnar microstructure on the corrosion damage of the whole TBC system and if a sealing layer that is relatively dense and has a compact microstructure on the

top can improve the performance of the coating. The double-layer GZ + YSZ/YSZ coating allowed the molten salts to infiltrate through its columnar gaps and reach the top coat/TGO interface. From the interrupted corrosion tests after 9 cycles, it was observed that the bond coat degradation was about 10% throughout the coating, except at the edges where severe bond coat degradation had occurred. The edge damage/degradation is due to the overflowing of the salts to the side surface, leading to a direct reaction with the substrate and the substrate/bond coat interface. As the side surface was not protected with any kind of coating, the damage is rapid. This damage from the edge subsequently propagates to the center of the coating. Degradation due to molten salt infiltration along with a rapid damage development from the edge thus resulted in corrosion damage observed in the double-layer system.

In the case of the triple-layer system with a relatively dense layer on the top, the corrosion mechanism is assumed to be the same as in the case of the double-layer TBC system. It must be noted that while the top layer in the triple-layer TBC was dense, there were still few vertical cracks (columnar gaps) in the coating which could not be avoided during the deposition of the TBCs. Due to the availability of fewer infiltration channels for the molten salts in the triple-layer system, most of the salts have overflowed to the edges. Due to the inert nature of gadolinium zirconate toward the corrosive salts, the salts could not be immobilized at the top surface. Thus, even with a similar mechanism for both the double- and triple-layer systems, the contribution of damage development from the edge seemed to be higher for the triple-layer system and, therefore, resulted in a relatively higher damage compared to the double layer. It has to be noted here that the large horizontal cracks in the triple-layer system may have occurred long before the tests were stopped and these delamination cracks can serve as an additional penetration channel for the molten salts.

As such, discarding the edge effect by applying some kind of protective coating to the side surfaces may result in similar behavior for the two coating systems. This is the subject of future research. Furthermore, an inert sealing layer may not be the optimum solution for reducing the corrosion damage. A reactive topcoat can restrict the salt infiltration to the upper parts of the coating. The results from the present investigation can be used as a general guideline during the design of coatings about the suitability of an inert sealing layer in the presence of molten salts.

Conclusions

Cyclic corrosion tests on a double-layer (GZ + YSZ/YSZ) and triple-layer (DGZ/GZ + YSZ/YSZ) SPS TBCs in the presence of a salt mixture of sodium sulfate and sodium chloride resulted in the following main conclusions.

1. The columnar gaps in the SPS coating served as effective pathways for the molten salt infiltration.
2. Due to the inert nature of the molten salts with the topcoat material, overflowing of the salts to the side surfaces occurred and resulted in damage development from the edge to the coating center.
3. The sealing layer in the triple-layer system proved to be ineffective due to the fact that the sealing layer reduced the number of infiltration channels for the molten salts and consequently, resulted in higher overflow of the salts and, thereby, relatively more damage.

Acknowledgments Vinnova in Sweden is gratefully acknowledged for funding this research.

Open Access This article is distributed under the terms of the Creative Commons Attribution 4.0 International License (<http://creativecommons.org/licenses/by/4.0/>), which permits unrestricted use, distribution, and reproduction in any medium, provided you give appropriate credit to the original author(s) and the source, provide a link to the Creative Commons license, and indicate if changes were made.

References

1. K. Vanevery, M.J.M. Krane, R.W. Trice, H. Wang, W. Porter, M. Besser, D. Sordelet, J. Ilavsky, and J. Almer, Column Formation in Suspension Plasma-Sprayed Coatings and Resultant Thermal Properties, *J. Therm. Spray Technol.*, 2011, **20**(4), p 817-828
2. W. Fan and Y. Bai, Review of Suspension and Solution Precursor Plasma Sprayed Thermal Barrier Coatings, *Ceram. Int.*, 2016, **42**(13), p 14299-14312
3. D.R. Clarke and S.R. Phillpot, Thermal Barrier Coating Materials, *Mater. Today*, 2005, **8**(6), p 22-29
4. M.J. Pomeroy, Coatings for Gas Turbine Materials and Long-Term Stability Issues, *Mater. Des.*, 2005, **26**(3), p 223-231
5. G.W. Goward, Progress in Coatings for Gas Turbine Airfoils, *Surf. Coat. Technol.*, 1998, **109**, p 73-79
6. N.P. Padture, M. Gell, and E.H. Jordan, Thermal Barrier Coatings for Gas-Turbine Engine Applications, *Science*, 2002, **296**, p 280-284
7. A. Thibblin, Thermal Barrier Coatings for Diesel Engines. Licentiate thesis, Kungliga Tekniska Högskolan, 2017
8. T.M. Yonushonis, Overview of Thermal Barrier Coatings in Diesel Engines, *J. Therm. Spray Technol.*, 1997, **6**(1), p 50-56

9. S. Mahade, N. Curry, S. Björklund, N. Markocsan, and P. Nylén, Thermal Conductivity and Thermal Cyclic Fatigue of Multilayered $Gd_2Zr_2O_7/YSZ$ Thermal Barrier Coatings Processed by Suspension Plasma Spray, *Surf. Coat. Technol.*, 2015, **283**, p 329-336
10. A. Ganvir, N. Curry, S. Björklund, N. Markocsan, and P. Nylén, Characterization of Microstructure and Thermal Properties of YSZ Coatings Obtained by Axial Suspension on Plasma Spraying (ASPS), *J. Therm. Spray Technol.*, 2015, **24**(7), p 1195-1204
11. N. Curry, K. VanEvery, T. Snyder, and N. Markocsan, Thermal Conductivity Analysis and Lifetime Testing of Suspension Plasma-Sprayed Thermal Barrier Coatings, *Coatings*, 2014, **4**, p 630-650
12. R. Vaßen, X.Q. Cao, F. Tietz, D. Basu, and D. Stöver, Zirconates as New Materials for Thermal Barrier Coatings, *J. Am. Ceram. Soc.*, 2000, **83**(8), p 2023-2028
13. X.Q. Cao, R. Vaßen, and D. Stöver, Ceramic Materials for Thermal Barrier Coatings, *J. Eur. Ceram. Soc.*, 2004, **24**(1), p 1-10
14. R. Vaßen, M.O. Jarligo, T. Steinke, D.E. Mack, and D. Stöver, Overview on Advanced Thermal Barrier Coatings, *Surf. Coat. Technol.*, 2010, **205**(4), p 938-942
15. D. Stöver, G. Pracht, H. Lehmann, M. Dietrich, J.-E. Döring, and R. Vaßen, New Material Concepts for the Next Generation of Plasma-Sprayed Thermal Barrier Coatings, *J. Therm. Spray Technol.*, 2004, **13**(1), p 76-83
16. B.R. Marple, J. Voyer, M. Thibodeau, D.R. Nagy, and R. Vaßen, Hot Corrosion of Lanthanum Zirconate and Partially Stabilized Zirconia Thermal Barrier Coatings, *J. Eng. Gas Turbines Power*, 2004, **128**(1), p 144-152
17. G. Mauer, M.O. Jarligo, D.E. Mack, and R. Vaßen, Plasma-Sprayed Thermal Barrier Coatings: New Materials, Processing Issues, and Solutions, *J. Therm. Spray Technol.*, 2013, **22**(5), p 646-658
18. A.V. Radha, S.V. Ushakov, and A. Navrotsky, Thermochemistry of Lanthanum Zirconate Pyrochlore, *J. Mater. Res.*, 2009, **24**(11), p 3350-3357
19. K.P. Jonnalagadda, S. Mahade, N. Curry, X.-H. Li, N. Markocsan, P. Nylén, S. Björklund, and R.L. Peng, Hot Corrosion Mechanism in Multi-layer Suspension Plasma Sprayed $Gd_2Zr_2O_7/YSZ$ Thermal Barrier Coatings In The Presence of $V_2O_5 + Na_2SO_4$, *J. Therm. Spray Technol.*, 2017, **26**(1–2), p 140-149
20. M.H. Habibi, L. Wang, and S.M. Guo, Evolution of Hot Corrosion Resistance of YSZ, $Gd_2Zr_2O_7 + YSZ$ Composite Thermal Barrier Coatings in $Na_2SO_4 + V_2O_5$ at 1050 °C, *J. Eur. Ceram. Soc.*, 2012, **32**, p 1635-1642
21. S. Mahade, K.P. Jonnalagadda, N. Curry, X.-H. Li, S. Björklund, N. Markocsan, P. Nylén, and R.L. Peng, Engineered Architectures of Gadolinium Zirconate Based Thermal Barrier Coatings Subjected to Hot Corrosion Test, *Surf. Coat. Technol.*, 2017, **328**, p 361-370
22. J. Ma, S.M. Jiang, J. Gong, and C. Sun, Hot Corrosion Properties of Composite Coatings in the Presence of NaCl at 700 and 900 °C, *Corros. Sci.*, 2013, **70**, p 29-36
23. Z.B. Bao, Q.M. Wang, Z.W. Li, X. Liu, J. Gong, T.Y. Xiong, and C. Sun, Preparation and Hot Corrosion Behavior of an Al-Gradient NiCoCrAlYSiB Coating on a Ni-Base Superalloy, *Corros. Sci.*, 2009, **51**(4), p 860-867
24. R.M. Leckie, S. Krämer, M. Rühle, and C.G. Levi, Thermochemical Compatibility Between Alumina and $ZrO_2-GdO_{3/2}$ Thermal Barrier Coatings, *Acta Mater.*, 2005, **53**(11), p 3281-3292
25. S. Mahade, N. Curry, S. Björklund, N. Markocsan, and P. Nylén, Failure Analysis of $Gd_2Zr_2O_7/YSZ$ Multi-layered Thermal Barrier Coatings Subjected to Thermal Cyclic Fatigue, *J. Alloys Compd.*, 2016, **689**, p 1011-1019
26. B. Cheng, G.-J. Yang, Q. Zhang, N. Yang, M. Zhang, Y. Zhang, C.-X. Li, and C.-J. Li, Gradient Thermal Cyclic Behavior of $La_2Zr_2O_7/YSZ$ DCL-TBCs with Equivalent Thermal Insulation Performance, *J. Eur. Ceram. Soc.*, 2018, **38**, p 1888-1896
27. V. Viswanathan, G. Dwivedi, and S. Sampath, Multilayer, Multimaterial Thermal Barrier Coating Systems: Design, Synthesis, and Performance Assessment, *J. Am. Ceram. Soc.*, 2015, **98**, p 1769-1777
28. X. Zhong, H. Zhao, C. Liu, L. Wang, F. Shao, X. Zhou, S. Tao, and C. Ding, Improvement in Thermal Shock Resistance of Gadolinium Zirconate Coating by Addition of Nanostructured Yttria Partially-Stabilized Zirconia, *Ceram. Int.*, 2015, **41**(6), p 7318-7324
29. R. Rampon, O. Marchand, C. Filatre, and G. Bertrand, Influence of Suspension Characteristics on Coatings Microstructure Obtained by Suspension Plasma Spraying, *Surf. Coat. Technol.*, 2008, **202**, p 4337-4342
30. K.P. Jonnalagadda, K. Yuan, X.-H. Li, X. Ji, Y. Yu, and R.L. Peng, Influence of Top Coat and Bond Coat Pre-oxidation on the Corrosion Resistance of Thermal Barrier Coatings in the Presence of SO_2 , *ASME. Turbo expo: power for land, sea and air, volume 6: ceramics, diagnostics, and instrumentation; education, manufacturing materials and metallurgy*, Oslo, Norway, 2018.
31. R.L. Jones, Some Aspects of the Hot Corrosion of Thermal Barrier Coatings, *J. Therm. Spray Technol.*, 1997, **6**, p 77-84
32. S. Rao, L. Frederick, and A. McDonald, Resistance of Nanostructured Environmental Barrier Coatings to the Movement of Molten Salts, *J. Therm. Spray Technol.*, 2012, **21**, p 887-899
33. A. Ravi Shankar, U. Kamachi Mudali, R. Sole, H.S. Khatak, and B. Raj, Plasma-Sprayed Yttria-Stabilized Zirconia Coatings on type 316L Stainless Steel for Pyrochemical Reprocessing Plant, *J. Nucl. Mater.*, 2008, **372**, p 226-232
34. H.-Y. Lee and K.-H. Baik, Comparison of Corrosion Resistance Between Al_2O_3 and YSZ Coatings Against High Temperature LiCl-Li₂O Molten Salt, *Met. Mater. Int.*, 2009, **15**, p 783-787
35. L.W. Zhang, X.J. Ning, L. Lu, Q.S. Wang, and L. Wang, Hot Corrosion Behavior of Low-Pressure Cold-Sprayed CoNiCrAlY Coatings, *J. Therm. Spray Technol.*, 2016, **25**(3), p 587-594
36. S.M. Jiang, Q.H. Li, J. Ma, C.Z. Xu, J. Gong, and C. Sun, High Temperature Corrosion Behavior of a Gradient NiCoCrAlYSi Coating II: Oxidation and Hot Corrosion, *Corros. Sci.*, 2010, **52**(7), p 2316-2322
37. Y. Shinata, Accelerated Oxidation Rate of Chromium Induced by Sodium Chloride, *Oxid. Met.*, 1987, **27**(5-6), p 315-332